Turn-on transient dynamics in a multimode, compound-cavity laser

S. E. Hodges,* M. Munroe, W. Gadomski,† J. Cooper,‡ and M. G. Raymer

Department of Physics and Chemical Physics Institute, University of Oregon, Eugene, Oregon 97403

Received September 21, 1995; revised manuscript received June 10, 1996

The turn-on-time statistics for an individual longitudinal mode and the total intensity of a multimode laser are shown to be very different. In both experiment and theory we find that the differences are due mainly to transitory modes that decay as a result of frequency-dependent losses and gains. Associated with this phenomenon is a kink in the time evolution of the mode intensity, but not in the total intensity, that represents a transition in the dynamics from domination by independent growth of all modes to domination by competition between modes with different net gains. This unequal competition increases the average and the standard deviation of the individual mode turn-on time. The experimental dye-laser system has a thin gain medium (100 μm) that is strongly coupled to a short cavity (2.5 cm) and is adjacent to one of the cavity mirrors. The opposite cavity mirror serves as a relatively weak output coupler. The presence of the thin gain medium in the cavity causes the effective pump and loss rates to be frequency dependent. The result is a transient spectrum in which the cavity modes that have the highest net gain dominate the system more as the turn-on transient progresses. The gain spectrum is found to be strongly affected by the frequency dependence of the compound-cavity modes. Using realistic laser parameters, numerical simulations of a multimode laser model {developed in companion paper [J. Opt. Soc. Am. B **14**, 191 (1997)]} yield turn-on dynamics and statistics that agree well with those measured experimentally. © 1997 Optical Society of America. [S0740-3224(97)01501-4]

1. INTRODUCTION

After a laser is connected to its power source there is a delay before a usable emission appears. The delay time, which is different every time the laser is powered up, is due to the laser's having a threshold for operation: For a laser to turn on, more atoms in the system must be stimulated to emit light than are required to compensate for losses, such as the laser output. Once threshold is exceeded, by exciting or pumping of the gain medium, the laser turns on and typically emits into the output beam many times more radiant energy than is present in the fluorescence glow (in the same solid angle) just below threshold. But, as is well known, the laser does not turn on instantly or predictably. Inasmuch as the turn-on is initiated by spontaneous emission—a random, quantum-mechanical process—the time that the laser takes to turn on varies randomly.

We describe the dynamics and statistics associated with the turn-on transient in a multimode laser. Previous research has studied the turn-on delay time (or first-passage time) statistics for the intensity in single-longitudinal-mode lasers,[1,2] in multimode lasers,[3–5] in modeless lasers,[6] and in lasers with injected signals.[7] The case of an M-mode laser in which all modes compete equally has been treated theoretically, yielding the prediction that the standard deviation of the turn-on time for the total intensity varies as $\sim 1/\sqrt{M}$.[8] Here we present and compare the turn-on time statistics for the total and the mode intensity in a standing-wave, multimode dye–laser system. Experimental and laser model simulation results are presented. The theoretical development of the laser model is described in a companion paper.[9]

The conclusion is that the total and the mode intensities develop differently. We present results that indicate that the turn-on transient of the intensity of an individual mode has two phases: an early one of rapid growth that is initiated by spontaneous emission and is independent of other modes, followed by a period of slow growth with dynamics dominated by competition with other modes for the finite reservoir of excited atoms, which leads to continuous wave (cw) operation. The simple $1/\sqrt{M}$ behavior is not followed because of the unequal competition between modes.

Figure 1 shows the averages of approximately 750 turn-on transients measured from a multimode dye-laser beam as a function of time after the pump is repetitively turned on (at TIME = 0) as described below. The pump and the total intensities and an individual mode intensity are shown. The total intensity turns on in a steplike fashion, as observed in previous turn-on transient studies.[10] Notice the change in slope in the mode intensity (indicated by the straight lines) coincident with the saturation of the total intensity (the vertical line). By this point in the transient behavior the mode intensity growth has become dominated by mode competition. The horizontal line through the mode trace indicates one standard deviation in the mode turn-on time (see below). The turn-on time is defined here as the time that the intensity takes to reach a certain fraction (e.g., 0.6) of the eventual cw level. The standard deviation for the total intensity turn-on time is ~1/100 that of an individual mode, approximately the thickness of the trace shown. This dramatic difference is a reflection of the nonlinear dynamics associated with mode competition. Similar results have been observed in numerical simulations of semiconductor lasers[11] and in the spectra of dye lasers.[12]

The system studied here is a standing-wave, multilongitudinal TEM_{00} laser with a short cavity: a short-cavity

0740-3224/97/010180-11$10.00

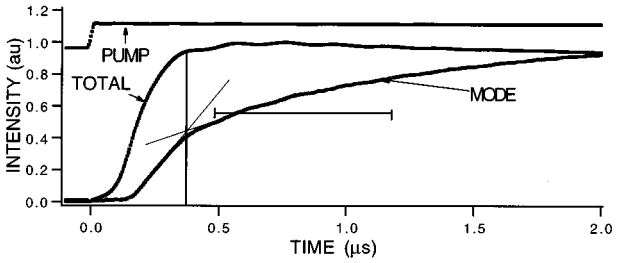

Fig. 1. Averages of experimental laser light intensities versus time. The mode and the total intensities are normalized; the pump intensity is calibrated by the laser threshold (at threshold, PUMP = 1.0 and TIME = 0.0). Approximately 750 turn-on transients are included in the averages shown. The vertical line indicates where the total intensity has saturated. The horizontal line through the mode trace indicates one standard deviation in the mode turn-on time.

dye laser (SCDL). We term the cavity "short" because the cavity loss rate (inversely proportional to the length of the cavity) is comparable with the spontaneous-emission rate (for mirror reflectivity ~95%). The gain medium of the laser acts as a weak intracavity étalon.[13] This phenomenon has an added effect on the already transient spectrum of a laser during its turn on: Modes on the edge of the profile as well as those that are not favored by the gain-medium étalon disappear in steady state.

To date an unanswered question is: How does the unequal gain competition among modes affect the fluctuations in the time that it takes for a mode intensity to build up to some given fraction of its eventual cw level? Turn-on time statistics for individual modes in a multimode laser were not calculated or measured previously. In this paper[14] we present such measurements for a multimode, coupled-cavity dye laser, determined both experimentally and theoretically. We hope that these results will further a deeper understanding of the laser process and help to refine developing laser models.

2. EXPERIMENTAL SETUP

Figure 2 shows the SCDL and the pump beam focused by a lens. The system is similar to that of the first cw dye laser demonstrated,[15] except that the output coupler of the system described here is a mirror external to the dye cell. The SCDL has a near-hemiconcentric cavity with a length of 2.5 cm. The 0.01-cm-thick $\sim 10^{-2}$ M Rhodamine 6G dye solution (index of refraction $n = 1.39$, pressure $\sim 5.7 \times 10^3$ Torr) flows between the flat mirror, where the beam waist forms, and a window that is antireflection (AR) coated on both sides (<0.5% reflectivity). The glass flat and the mirror substrates are 1-cm-thick BK-7 glass with one side wedged ~5 min from parallel with respect to the other side, thus reducing unwanted reflections. The pressure fluctuations of the dye fluid are reduced to less than 10 Torr, peak to peak, by use of a pressurized diaphragm damper and a backpressure valve, which minimizes unwanted laser dynamics that are due to the pressure fluctuations of the dye fluid.[16] The pump is a cw argon-ion laser with a single-longitudinal-mode TEM_{00} output at 514 nm. Working close to the SCDL threshold requires that the pump laser's intensity be stabilized to much less than the intrinsic 10% peak-to-peak fluctuations.[17,18] The pump laser is intensity stabilized with an external-feedback electro-optic noise eater, resulting in ~0.5% peak-to-peak fluctuations when they are monitored by a 1-GHz-bandwidth detector.

The argon-ion laser light is repeatedly pulsed at a 10-Hz rate from below the SCDL threshold (nominally at 250 mW) to the desired pump rate with an ~20-ns rise time, little or no ringing, and an ~8-μs duration, with an electro-optical modulator. A beam splitter reflects less than 1% of the pump light to a silicon detector to monitor and stabilize actively the pump pulses generated by the electro-optical modulator.

The prepulse pump rate is 1–2% below threshold to minimize optical distortions owing to thermal effects in the dye when the pump rate is increased. The effects arise from the thermal dispersion of the dye mixture's index of refraction. The pump pulse heats the dye inhomogeneously so that an index gradient, and thus a thermal lens, forms. The time dependence of such acousto-optical distortions can be quite complicated and typically requires several microseconds to stabilize.[19] These effects are minimized by use of appropriate dye solvent recipes at a temperature where the thermal dispersion is minimal.[5,20] The recipe that we use is 2.0 g of Rhodamine 590 tetrafluoroborate dissolved in a solution comprising 1.0 L of methanol, 3.6 L of Ammonyx, and 4.4 L of distilled water. The best performance is achieved when the dye solution is cooled to 5 ± 3 °C.

The thermal burden on the dye is reduced, and increased pumping efficiency is achieved, by choice of a pump focusing lens that mode matches the pump with the dye laser cavity. The achromatic lens used has a focal length of 3.0 cm and is AR coated. The resulting dye and pump laser waists are ~10 μm, measured by observation of the far-field pattern.

The SCDL total emission power (at $\lambda \approx 590$ nm) is ~10 mW at 10% above threshold. Approximately 5% of this emission is measured with a silicon photodiode after being deflected by a coated pellicle beam splitter. We call this signal the total intensity. The rest of the SCDL light enters a 0.35-m grating monochromator, where it is spectrally resolved and measured with a photomultiplier with 16% quantum efficiency. The monochromator is tuned to a wavelength on or near the peak of the emission spectrum. We call this signal the mode intensity because the monochromator bandwidth equals approximately five cavity mode spacings.

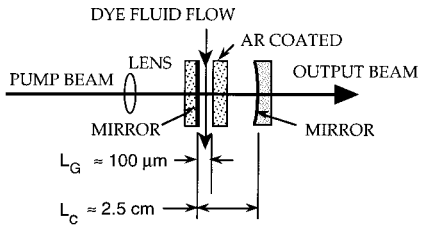

Fig. 2. SCDL showing the dye cell, the external mirror, and the pump lens.

The total, mode, and pump intensity signals are digitized (with 12-bit precision) at a 250-Msample/s rate by a digital oscilloscope. Waveforms of 2048 points are downloaded to a computer at a rate of ~3/s, where they are stored for later processing. The limiting analog bandwidth for all acquisitions is ~100 MHz.

A. Procedure

In cw operation the SCDL emission spectrum, observed with limited resolution, consists of several peaks separated by a wavelength interval of 1.4 nm. This interval corresponds to the free spectral range of an intracavity étalon formed by the gain medium. The monochromator resolution is ~0.02 nm, approximately 1/50 of the free spectral range set by the gain medium and roughly five laser-cavity mode spacings. To measure the mode intensity we tune the monochromator to one of the cw spectral peaks near the center of the spectrum.

The experimental procedure consists of collecting ~10 waveforms for several pump rates and repeating this step until roughly 1000 pulses at each pump rate have been recorded. In this way the stability of the SCDL can be monitored and the excess pump rate (amount above threshold) can be determined to within ±1%. Timing information is extracted from the waveforms by use of the averaged pump data as a zero-time reference. The pump pulse timing jitter is less than 100 times smaller than the intrinsic jitter of the SCDL signals. The turn-on time of a given waveform is measured with respect to a fraction of its cw level for each pulse. The goal is to determine the average, the standard deviation, and the skew of the times to build up to various fractions of the cw level.

We measure the spectrum of the SCDL emission by sampling the photomultiplier signal, using a boxcar integrator, and slowly scanning the monochromator. The boxcar is set to sample during a small period of time within the SCDL output pulse (typically a 10-ns-wide window). The sample interval is fixed either in the turn-on period or in the cw period of the laser action.

The SCDL output intensity and spectrum are highly sensitive to wavelength-scale changes in the distance between the external mirror and the gain medium, as has been demonstrated theoretically[21] and experimentally.[22] Before measuring turn-on transients for statistical analysis, we align the SCDL so that the cw output spectral peaks, when imaged from a holographic grating (1200 mm^{-1}), form an unmodulated and symmetric envelope. This procedure results in reproducible turn-on time statistics.

B. Raw Data

Figure 3 shows measured SCDL turn-on transients and spectra. Approximately 150 turn-on events of the total intensity and in two regions of the SCDL emission spectrum are shown in traces (a)–(c) of Fig. 3. Two spectra are shown in traces (d) and (e). Trace (d) is sampled early in the turn-on (0.25 μs ns after the SCDL is above threshold); trace (e) is sampled after the laser has become cw (5.5 μs after going above threshold). The mode shown in trace (b) corresponds to a central peak, which becomes stable in the cw regime. The mode shown in trace (c) corresponds to an edge peak that does not survive the turn-on transient.

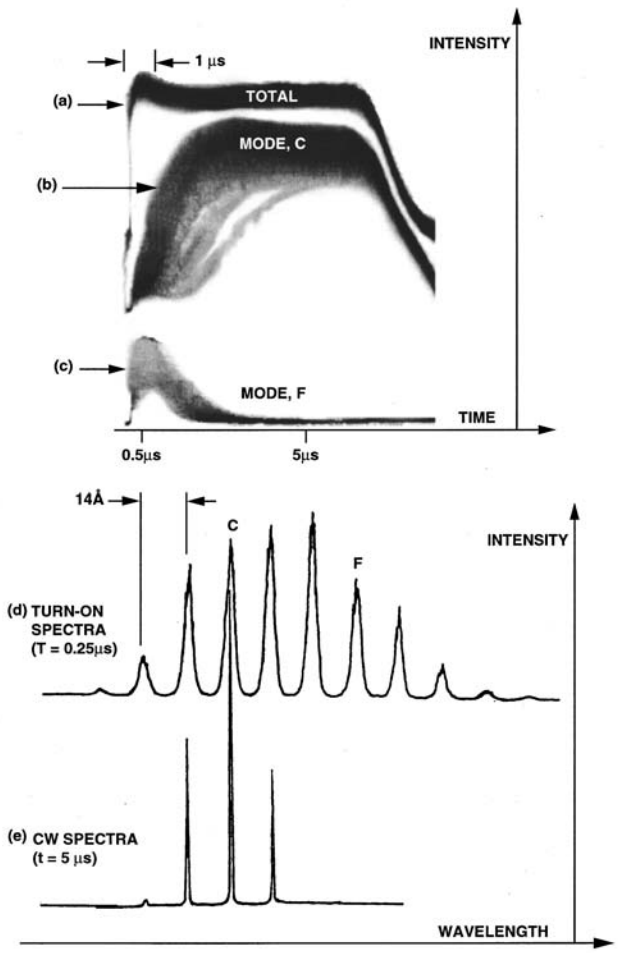

Fig. 3. Approximately 150 turn-on transients for (a) the total intensity, (b) the center spectral peak C, and (c) a fringe spectral peak F that does not survive the turn-on transient. Also shown are SCDL spectra sampled in a 10-ns window (d) while the laser is turning on, 0.25 μs after the SCDL is above threshold, and (e) while the laser is operating cw.

A key point is that the distance between the spectral peaks in traces (d) and (e) of Fig. 3 is given by the inverse of the gain medium length, not by the cavity length. Evidently the net gain is highest for modes that most closely match the weak boundary condition introduced by the (low-finesse) étalon formed by the intracavity gain medium. We make this argument rigorous by deriving mode functions for the compound-cavity geometry[12] and applying them in the laser equations, as is done in the simulations described below. The net gain is thus found to be modulated in frequency, as one might intuitively expect from traces (d) and (e) of Fig. 3.[13,22]

The differences in the total intensity and the mode intensity turn-on transients that are evident in Fig. 3 can be further illuminated by time resolution of the spectrum, as presented in an earlier publication.[4]

3. EXPERIMENTAL TURN-ON TRANSIENT STATISTICS

A. Statistical Algorithms

The experiment described above generated thousands of intensity-versus-time traces for the SCDL operated at various pump levels. These data were reduced statistically, resulting in measurements of the first three moments of the turn-on times. Here, turn-on time is defined as the time t_f required for the total or mode intensity to reach a reference fraction f of its ultimate cw intensity on a particular pulse. Thus the probability-density function (pdf) for the laser turn-on delay time is determined at several points during the laser turn-on.

The average $\bar{t}_f$, the standard deviation Δt_f, and the skew s_f associated with the pdf are determined by use of the following equations[23]:

$$\bar{t}_f = \frac{1}{N}\sum_{j=1}^{N} t_f(j), \tag{3.1}$$

$$\Delta t_f = \left\{ \frac{1}{N-1}\sum_{j=1}^{N} [t_f(j) - \bar{t}_f]^2 \right\}^{1/2}, \tag{3.2}$$

$$s_f = \frac{1}{N}\sum_{j=1}^{N} \left[\frac{t_f(j) - \bar{t}_f}{\Delta t_f} \right]^3, \tag{3.3}$$

where j is the pulse number and N is the total number of pulses measured for a given experimental configuration (i.e., a fixed pump level).

The uncertainty (i.e., spread) in the measured turn-on times is given by the standard deviation. The skew measures the symmetry of the pdf as a function of the independent variable (t_f) and so gives some idea of how the variable is distributed about the pdf maximum. A perfectly symmetric pdf (e.g., a Gaussian distribution) has zero skew. When the pdf maximum occurs at a t_f less (greater) than the average, the skew is positive (negative).

B. Experimental Data Reduction

In the experiment five nominal pump levels are used, with the lowest being close to threshold. From these data a least-squares line is fitted to the total-versus-pump intensity so the pump level is calibrated in terms of the SCDL threshold. Figure 4 shows a scatter plot of the cw level of the total intensity plotted versus the cw level of the pump intensity for the (calibrated) pump levels. Only pulses for which the pump level falls within ±1/2% of each nominal value are processed. The zero slope within each pump level group is due to pump digitization error: The width of each group of points is equal to the 1% resolution of the pump measurement. Approximately 750 pulses are used for computing the statistics at each pump level.

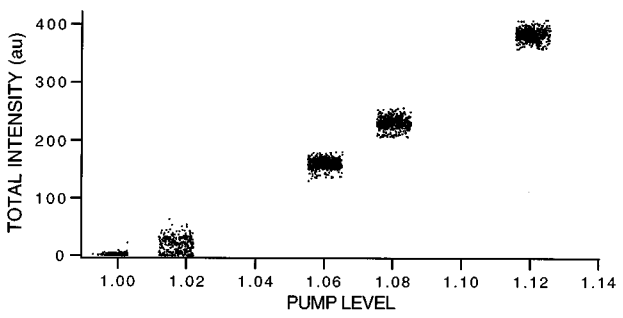

Fig. 4. Total intensity cw value plotted versus calibrated cw pump levels.

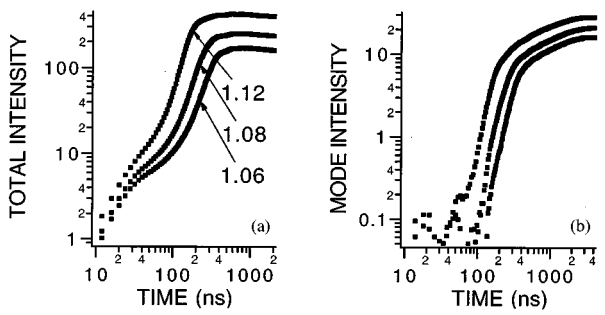

Fig. 5. (a) Averaged total intensity and (b) averaged center cw mode intensity versus time for three pump levels: 6%, 8%, and 12% above threshold.

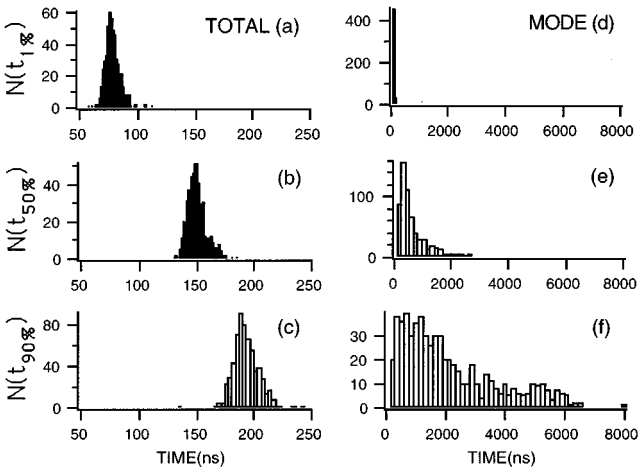

Fig. 6. Histograms of the turn-on times to (a), (d) 1%; (b), (e) 50%; (c), (f) 90% of the cw level for the total intensity and the center cw mode intensity for a pump level of 1.12.

Figure 5 shows the averaged intensity of the total and the cw mode at the center of the spectrum (the center cw mode, C) versus time, measured with the SCDL operating 6%, 8% and 12% above threshold.

Figure 6 shows histograms (50 bins, uniformly distributed for each data set) of the turn-on times measured for the 1.12 pump level to several reference levels. Note the different horizontal time scales for the mode and the total intensity data. The histograms are approximately equal to the pdf for the turn-on time, t_f. The total intensity results [Figs. 6(a)–6(d)] are similar to those reported by Zhu *et al.*[2] Differences between the transient behavior of the center cw mode [Figs. 6(e)–6(h)] and of the total intensity are evident in the distribution of times early and late in the turn-on: At early stages (less than 10% of the cw level)

the times are well grouped in both cases, whereas late in the turn-on (beyond ~10% of the cw level) the mode times are distributed over a relatively broader range than are the total intensity times. These differences are made quantitative below, in Figs. 10–12, where the average, the standard deviation, and the skew of the turn-on times to various reference levels are shown for the center cw mode and total intensities.

4. LASER MODEL

The companion paper[9] presents a laser model that we now apply to the experimental system described above. This model is a refinement of the one that we used to analyze the experimental results in Ref. 4, as it uses the coupled-cavity modes that were developed later.[13] Specifically, we simulate the class-B laser equations (4.8)–(4.12) of Ref. 9. Here we neglect the coherent coupling (i.e., $p \neq 0$) terms and the associated mode noise correlations as well as the precise form of the inversion noise correlations suggested by Eqs. (4.11) and (4.12) of Ref. 9. The detuning between the atoms and the cavity is assumed to be zero; $\delta = 0$ in Eq. (5.4) of Ref. 9. Also, the cavity mirror reflectivity $\Re$ and the interface reflectivity r are assumed not to vary with frequency, as is the pump rate R (see Fig. 7). In simulations in which the pump is spatially uniform and the mode functions have the plane-wave form $u_j(z) \approx A_j \sin(nj\pi z/L_C)$, the spatial overlap integral of the pump rate R is given by Eq. (3.13) of Ref. 9, yielding $R^0_{j,k} \approx RnL_G|A_j|^2\delta_{j,k}/2$ for the pump rates of the spatial components of the population inversion. Here n is the index of refraction of the gain medium, L_G is the optical length of the gain medium, and L_C is the optical length of the cavity. Thus only the diagonal population terms ($j = k$) are pumped. Therefore the off-diagonal terms $W^0_{j,k}$ of the spatial overlap of the inversion $W(z)$ are relatively small and so can be neglected. Because only the diagonal inversion and noise terms remain, we simplify the notation by representing the remaining terms of the inversion overlap $W^0_{j,j}$ and the field noise F^j_j with a single index (i.e., $W^0_{j,j}$ becomes W_j and F^j_j becomes F_j). The noises are assumed to be Gaussian random variables when they are written in differential form suitable for numerical calculations (i.e., F_j becomes $\mathrm{d}F_j$) by the methods described by Gardiner.[24] The correlations between the field noises $\mathrm{d}F_j$ of different modes that are due to coherent coupling [see Eq. (4.11) of Ref. 9] are neglected (i.e., $\langle \mathrm{d}F_j \mathrm{d}F_k \rangle = 0$ if $j \neq k$). The equations for the complex mode field amplitudes E_j and inversion overlap integrals W_j, written as the differentials that are used in the simulations that follow, now read as

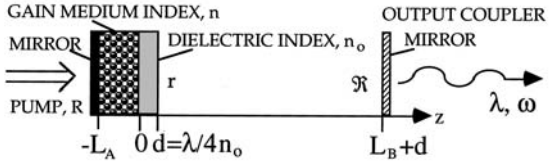

Fig. 7. Compound-cavity laser system.

$$\mathrm{d}E_j(t) = \left[\frac{g_j^2}{\beta_j} W_j(t) - \frac{1}{2}\kappa_j\right] E_j(t)\mathrm{d}t + \sqrt{8\pi\hbar\omega_j}\,\mathrm{d}F_j(t), \tag{4.1}$$

$$\mathrm{d}W_j(t) = \left\{ \gamma_\parallel [R_j - W_j(t)] - \frac{\mu^2}{2\gamma_\perp \hbar^2} \times \sum_m \alpha_{j,j,m,m} l_m |E_m(t)|^2 W_m(t) \right\} \mathrm{d}t + \mathrm{d}G_j(t). \tag{4.2}$$

Here the polarization damping rate is $\beta_j = \gamma_\perp + i(\omega_j - \omega_{21})$, κ_j is the mode intensity loss rate, $\gamma_\parallel$ is the population decay rate, and $\alpha_{j,j,m,m}$ is the overlap integral of four mode functions over the gain medium representing mode competition [Eq. (3.15) of Ref. 9]. The field–matter coupling constant is $g_j^2 = 2\pi\mu^2\omega_j/\hbar$, where μ is the dipole moment of the transition, the laser line-shape function is $l_j = \gamma_\perp^2[\gamma_\perp^2 + (\omega_j - \omega_{21})^2]^{-1}$, ω_j is the frequency of the jth mode, ω_{21} is the optical frequency of the lasing transition, and $\gamma_\perp$ is the collisional dephasing rate of the molecular dipoles. The time step of the integration is $\mathrm{d}t$. The complex field noise $\mathrm{d}F_j$ has a variance, found from Eq. (4.11) of Ref. 9, that is equal to $2g_j^2 l_j \bar{W}_j \mathrm{d}t/\gamma_\perp$. We show below that $\bar{W}_j = \kappa_j\gamma_\perp/2g_j^2 l_j$, which yields[24]

$$\mathrm{d}F_j = \kappa_j \mathrm{d}t. \tag{4.3}$$

The (real) inversion noises $\mathrm{d}G_j(t)$, given in Eq. (4.12) of Ref. 9 are correlated by the intrinsic inversion component noises $\theta_{j,k}(t)$. They also contain off-diagonal field noises $F_m^{q\neq m}(t)$ that appear nowhere else in the theory. To simplify the simulation enough that statistically significant data can be generated, the diagonal intrinsic inversion noise components $\theta_{j,j}(t)$ are taken to be the same for distinct modes, i.e., $\theta_{j,j}(t) = \theta_{k,k}(t)$. This assumption is reasonable inasmuch as the molecular noise should contribute roughly the same to adjacent modes. Furthermore, the off-diagonal field mode noises are neglected. The differential form of the inversion noise is then

$$\mathrm{d}G_j(t) = \mathrm{d}\Theta - \frac{\mu}{2\hbar} \sum_m \frac{\alpha_{j,j,m,m}}{g_m} [E_m^*(t)\mathrm{d}F_m(t) + E_m(t)\mathrm{d}F_m^*(t)], \tag{4.4}$$

where $\mathrm{d}\Theta$ is a Gaussian random variable with a variance of $2\gamma_\parallel \mathrm{d}t/\rho$ (where ρ equals the density of gain centers) and represents the intrinsic noise that is due to fluctuations of the inversion population. The effects of the neglected correlations are expected to be insignificant in the case considered here because coherent mode coupling effects are small. Future studies may find significant effects that result from these off-diagonal inversion noise correlations, especially in systems in which coherent coupling effects, e.g., four-wave mixing, are dominant.

The pump rate at threshold is precisely the steady-state inversion $\bar{W}_j$, so an arbitrary pump rate is given by $R_j = (1 + x)\bar{W}_j$, with x being the fraction of the pump level beyond the laser threshold. Because the phase of E_j may fluctuate when the field amplitude is in steady state, one must write Eq. (4.1) as an intensity ($I_j = |E_j|^2$) equation to find $\bar{W}_j$. The result (neglecting the noise) is

$$dI_j(t) = \left[\frac{2g_j^2 l_j}{\gamma_\perp} W_j(t) - \kappa_j\right] I_j(t)dt. \tag{4.5}$$

Setting the left-hand side of Eq. (4.5) to zero yields $\bar{W}_j = \kappa_j\gamma_\perp/2g_j^2 l_j$, so the pump level is given by

$$R_0 = (1 + x)\frac{\kappa_0\gamma_\perp}{2g_0^2 l_0} \tag{4.6}$$

for the center mode. Laser threshold corresponds to $x = 0$.

We now apply Eqs. (4.1)–(4.4) to the case of lasers with compound cavities.

A. Compound-Cavity Laser Simulation

Since the publication of Ref. 4 we have developed a solution for the modes of a coupled-cavity laser appropriate to the dye laser under study. The solution is briefly reviewed here. Consider a partially filled cavity, as in Fig. 7, with the gain medium adjacent to the left-hand mirror and with $L_B \neq 0$, for which the modes are significantly different from those in a filled-cavity case ($L_B = 0$). Note that L_G and L_C are optical lengths, whereas L_A and L_B are physical lengths: $L_G = nL_A$ and $L_C = L_B + (n_0 - 1)d + nL_A$, where n is the refractive index of the gain medium (related to the dielectric constant by $\epsilon = n^2$), and d is the thickness of the dielectric layer (see Fig. 7).

The quarter-wavelength-thick dielectric layer of index n_0 allows the reflectivity r to be different from the Fresnel reflection that is due to the gain medium index n and the empty-cavity index 1 (see Ref. 25). The index n_0 can be imagined to have a dispersion such that it is optically one quarter of a wavelength thick for all frequencies of interest (or a multilayer dielectric stack can be explicitly considered; see Chap. 1 of Ref. 25). The intensity reflectivity r is related to n and to n_0 by

$$r = (1 - J)^2/(1 + J)^2, \tag{4.7}$$

where $J = n_0^2/n$. We can show this easily by removing the mirrors in Fig. 7 and considering a wave incident upon the gain-medium side, partially reflected from the dielectric with the remainder transmitted through the dielectric. The intensity transmittivity t is given by $1 - r$. When $n_0 = n$ ($J = n$) the usual Fresnel result is obtained. A perfect AR coating is modeled with $n_0 = \sqrt{n}$ ($J = 1$); in this case $r = 0$ and $t = 1$.

Numerically simulating Eqs. (4.1)–(4.4) requires that functional forms for the spatial mode functions $u_q(\mathbf{r})$ be specified so that the overlap integrals of $\alpha_{p,p,q,q}$, κ_q, and R_q can be evaluated. When the reflectivity of the output coupler $\Re \approx 1$, the spatial mode functions for the compound, coupled-cavity laser shown in Fig. 7 have the (one-dimensional) form

$$u_q(z) = \begin{cases} A_q \sin[k_q n(z + L_A)] & -L_A \leq z \leq 0 \\ C_q \exp(ik_q n_0 z) + \text{c.c.} & 0 \leq z \leq d \\ B_q \sin[k_q(z - L_B - d)] & d \leq z \leq L_B + d \end{cases}, \tag{4.8}$$

where $k_q = \omega_q/c$.

We find expressions for A_q and B_q by applying the boundary conditions for the electric and magnetic fields given by classical electrodynamics and demanding orthonormality as in Eq. (3.3) of Ref. 9. The boundary conditions are that the functions $u_q(z)$ and their first derivatives $du_q(z)/dz$ be continuous across the two dielectric interfaces shown in Fig. 7. In Ref. 13 a useful (approximate) result is shown to be (for $nL_A, L_B \gg \lambda$)

$$A_q^2 = \frac{2}{L_B}\left[\frac{\alpha_E J/n}{1 + \alpha_E(J^2 - 1)\sin^2(k_q nL_A)}\right], \tag{4.9}$$

$$B_q^2 = \frac{2}{L_B}\left[1 - \frac{\alpha_E JnL_A/L_B}{1 + \alpha_E(J^2 - 1)\sin^2(k_q nL_A)}\right], \tag{4.10}$$

where $\alpha_E = (1 + JnL_A/L_B)^{-1}$. Note that Eqs. (4.9) and (4.10) are Airy formulas, familiar in the theory of resonant cavities.[27]

In the case when the output coupler is on the opposite side of the cavity from the gain medium, as in the experiment described here, the field loss rate, [Eq. (3.17) of Ref. 9] is given by

$$\kappa_q = c(1 - \Re)B_q^2/4. \tag{4.11}$$

Similarly, the pump parameter, which we find from Eq. (3.13) of Ref. 9 by using the derived spatial mode functions, is given by

$$R_q = nRL_G A_q^2/2. \tag{4.12}$$

Thus the pump level R_q is modulated in mode index q (i.e., frequency) so the modes that most closely match the boundary conditions of the gain medium have the highest pumping. Inasmuch as the gain term in Eq. (4.1) is proportional to pump level R_q, the mode with the highest pumping will have the highest gain. This quantitatively explains the free spectral range of the strongly lasing peaks observed in traces (a) and (e) of Fig. 3. Note from Eqs. (4.11) and (4.12) that the gain modulation with mode number is much larger than the loss modulation, contrary to the intuitive assumptions that experience with passive étalons may lead to.

Finally, for $L_G \ll L_C$ the spatial mode overlap integral of Eq. (3.15) of Ref. 9 is given by

$$\alpha_{j,j,m,m} = \epsilon A_j^2 A_m^2 L_G \frac{1}{4}\left\{1 + \frac{\sin[2\pi(j - m)L_G/L_C]}{4\pi(j - m)L_G/L_C}\right\}. \tag{4.13}$$

The behavior of this spatial overlap shows that the cross-saturation effects cause coupling most strongly between modes that are near in frequency.

B. Dynamical Simulations

Using the mode functions given by Eqs. (4.9) and (4.10), we numerically modeled the coupled-cavity system of Fig. 7 by solving Eqs. (4.1) and (4.2), using Eqs. (4.3) and (4.4) to specify the noise. Random numbers for the noises are generated with the subroutine GASDEV given by Press *et al.*[23] The modes included in the calculation are shown in Fig. 8. The 91 modes are separated into seven groups of 13 modes each. The center mode group is labeled C, the intermediate group is labeled I, the edge group E is the farthest from line center that survives the turn-on transient, and the fringe group that does not survive the turn-on transient is labeled F. The separation of the groups is proportional to the inverse of L_G; the separation of modes within each group is proportional to $1/L_C$.

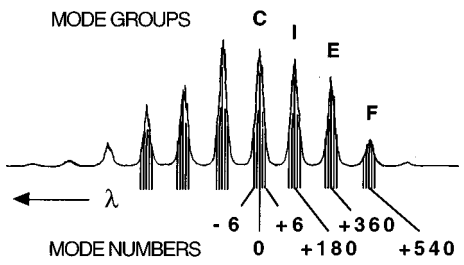

Fig. 8. Illustration of mode groups and modes included in the coupled-cavity simulation, superposed upon the measured SCDL spectrum of trace (d) of Fig. 3.

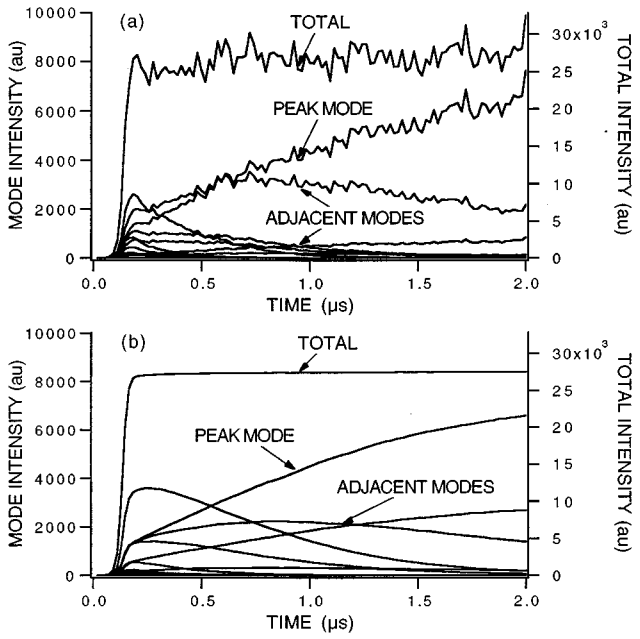

Fig. 9. Single-pulse simulation results for the total intensity and the intensities of the center group of 13 modes (a) with and (b) without inversion noise included in the simulation. Labeled are the peak mode, which is at the center frequency of the mode group, and the two modes adjacent to the center.

The mode frequency (rad/s) is given by the mode number j of Fig. 8 by $\omega_0 + j\pi c/L_C$, where ω_0 is the frequency at the center of the spectrum.

In the simulations that follow, the initial conditions (at $t = 0$) of the field and inversion correspond to a pump level that is 2% below threshold, i.e., $x = -0.02$, to model the experimental procedure described above. The collisional dephasing rate $\gamma_\perp$ is tweaked so that the numerical simulations produce the same number of lasing modes as observed experimentally. The output coupling reflectivity $\Re$ (and thus the cavity loss rate κ_j) is adjusted so that the simulated and experimentally observed center-mode turn-on delay times to 1% of the cw mode intensity agree.

Figure 9 shows one simulation of the total intensity and several mode intensities versus time for a pump level of 12% above threshold and an interface reflectivity $r = 0.07$. Figure 9 shows the results including or excluding the inversion noise dG_j, [Eq. (4.4)]. The field noise dF_j in Eqs. (4.1) and (4.3) is included in both of the simulations. The mode traces shown correspond to the center group C (13 of 91 modes). The parameters used in the simulations discussed below are gain-medium length $L_A = 0.01$ cm, external-cavity length $L_B = 2.5$ cm, mode waist $w_0 = 0.001$ cm, output coupler reflectivity $\Re = 0.88$, collisional dephasing rate $\gamma_\perp = 1.0 \times 10^{14}$ s^{-1}, gain-medium index $n = 1.39$, dipole moment $\mu = 2.4 \times 10^{-18}$ (erg cm^3)$^{1/2}$, population decay rate $\gamma_\parallel = 5.0 \times 10^8$ s^{-1}, center optical frequency $\omega_0 = 3.2 \times 10^{15}$ s^{-1}, and density of gain centers $\rho = 1.0 \times 10^{18}$ cm^{-3}.[28] One 10,240-point simulation including 91 modes (i.e., 7 groups of 13 modes) and spanning ~18 μs requires ~570 s of computation time on a DEC 3000 workstation.

It is interesting to compare Fig. 9(a), which includes the inversion noise dG_j of Eq. (4.4), with Fig. 9(b), where dG_j is set to zero in the simulation. In both cases it is the field noise dF_j that is responsible for the initiation of lasing. Nevertheless, it is clear that the inversion noise cannot be neglected in general. We point out that the intrinsic inversion noise $d\Theta$ in Eq. (4.4) contributes roughly half of the noise apparent in the total intensity trace of Fig. 9(a), whereas the remaining noise originates from the atomic polarization noise (manifested in the field noise; see Ref. 9).

In the simulations, different modes appear to dominate different turn-on events.[5] Fewer modes appear to be involved in this mode hopping as r is increased, as one might intuitively expect by considering the frequency-dependent gain of the coupled cavity. Also, although the laser remains multimode, a single mode tends to lase in each mode group for the larger reflectivity. In all cases little lasing action is observed in the mode group farthest from the center of the line shape, indicating that seven groups is a reasonable choice. The laser appears to operate single mode at 2% above threshold.

Critical slowing of the intensity in the simulated class-B system was observed[5] that was similar to that in the class-A case considered by Yu *et al.*[17] We use this behavior in the simulations to choose the most efficient calculation time step dt.

5. COMPARISON OF EXPERIMENT AND THEORY

A. Composite Modes

We now present the turn-on time statistics obtained from the simulations and compare them with the experimental results. To calculate the statistics of the data from the simulations we apply the same statistical algorithms that were used to reduce the experimental data. The parameters used are the same as those given in Subsection 4B. Because the turn-on behavior is seen to depend sensitively on the interface reflectivity r in the simulations[5] we choose the value $r = 0.07$, which yields the best fit with the experimental results. This is substantially higher than the corresponding reflectivity of the AR-coated glass flat. This discrepancy could be due to the presence of optical absorption or scattering by dye impurities deposited upon this interface surface, which would enhance the

modulation of the net gain (gain minus loss) with mode number, similar to the effect of increasing r.

Figure 10 compares the average of the turn-on times of the theoretical simulation and the experiment when the laser is 12% above threshold. The results are given for the total and the mode intensities versus the reference intensity level (the fraction of the ultimate cw intensity). Results are shown for the peak mode of the center group C and for a so-called mode that is computed as the sum of the intensities of the peak mode and its two adjacent modes, hereafter called a composite mode. This models the experimental situation, in which the mode intensity was measured with a monochromator resolution of approximately three to five cavity mode spacings, so the measured signal is the sum of several modes. Approximately 750 turn-on events are used to generate the statistics in both the simulations and the experiment.

Figures 11 and 12 compare the standard deviation and the skew of the turn-on times of the experiment and the simulation. Again, the laser is 12% above threshold. The agreement between the experimental and the simulation turn-on time statistics for the total and the composite-mode intensities shown in Figs. 10–12 is quite good. The increasing slope in the average turn-on time of the composite mode corresponds to the kink in the intensity-versus-time data in Fig. 1 and curve (b) of Fig. 3. This behavior is not seen in the simulations if only the cw modes are included and the adjacent, transitory modes are excluded.[4] Furthermore, the standard deviation of the composite-mode turn-on time is greatly underestimated by the simulations when these transitory modes are excluded.[4] This finding strengthens our interpretation that the kink behavior is due to the onset of mode competition through cross saturation and the frequency dependence of the coupled-cavity gain. The discrepancy in the average turn-on time of the total intensity for a small reference fraction, i.e., early in the turn-on, is expected to be sensitive to the number of modes (91) used in the simulation because at small times all 1000 modes begin to turn on. Simulating too few modes would have less effect on the simulated mode dynamics because the modes that becomes cw are influenced mainly by other modes most similar in frequency. The fact that the experimental result for the total intensity turn-on time standard deviation is larger than that in the simulation is likely due to the presence of pump fluctuations in the experiment. The origin of the large discrepancy of the total intensity turn-on time skew at the point reference intensity fraction of 0.2, shown in Fig. 12, at late stages of the turn-on transient is unclear.

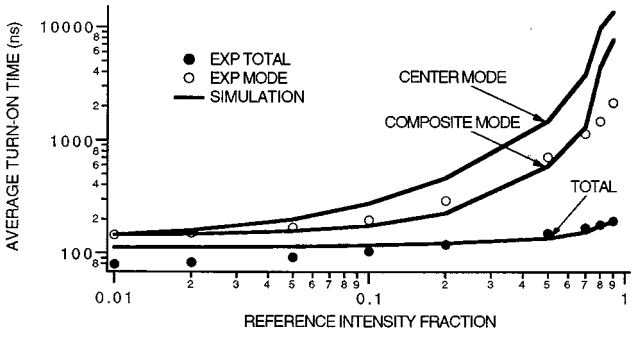

Fig. 10. Average turn-on time versus the fraction of cw intensity for the total and the mode intensities measured from the experiment (EXP) at 12% above threshold. Results for the simulated total, peak, and composite-mode intensities are also shown.

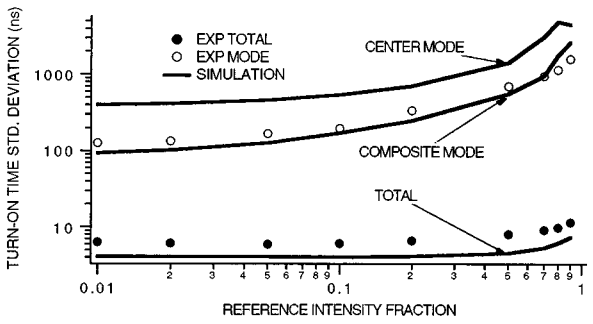

Fig. 11. Standard deviation of turn-on time versus the fraction of cw intensity for the total and the mode intensities measured from the experiment (EXP) and the simulation.

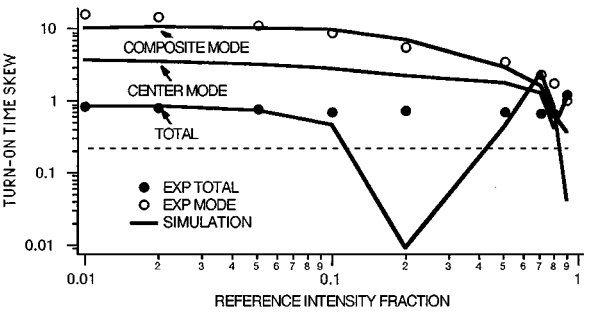

Fig. 12. Skew of the turn-on time versus the fraction of cw intensity for the total and the mode intensities measured from the experiment (EXP) and the simulation. The dashed line corresponds to the maximum skew expected from a symmetric density function based on 750 samples ($6/\sqrt{N}$).

One can understand the larger skew evident in Fig. 12 for the mode turn-on times for small reference intensities, compared with that for the total intensity, by considering the early growth of the intensity $I(t)$ of a laser mode:

$$I(t) = I(0)\exp(Gt), \tag{5.1}$$

where G is the gain coefficient and $I(0)$ represents the spontaneous emission that seeds the laser mode. For illustrative purposes we represent $I(0)$ as a random variable $I(0) = I_0(1 + \delta)$, where $I(0)$ has an average value of I_0 and a fractional deviation of δ. If we define $i(t) = I(t)/I_0$, then $i(t) = (1 + \delta)\exp(Gt)$. At time t_f, $i(t_f) = F$ (here $F > 1$ is a reference level) and

$$t_f = \frac{1}{G}\ln\left(\frac{F}{1 + \delta}\right). \tag{5.2}$$

The average number of spontaneously emitted photons (i.e., I_0) in a laser mode is 1. The standard deviation, given by the square root of the average, is also 1. Thus δ

typically ranges from +1 to −1. When δ is close to −1, t_f is large. When δ is close to +1, t_f is not significantly different from that when $\delta = 0$. Thus a symmetrically distributed seed amplitude gives rise to an asymmetric distribution of turn-on times. This is the origin of the large skew in the mode turn-on time statistics.

The pdf of the total intensity turn-on time is not so skewed as that of the mode intensity because the total intensity is composed of many modes: more than 1000 are observable in the experimental system. Thus the standard deviation of the total intensity seed is relatively small compared with the average seed [i.e., $\delta \ll 1$ in Eq. (5.2)].

B. Effect of the Intrinsic Inversion Noise

Figures 13 and 14 compare the experimental and the composite-mode simulation data shown in Figs. 10 and 11 with the results of a composite-mode simulation in which the inversion noise, dG_j of Eqs. (4.2) and (4.4), is set to zero. All other simulation parameters are unchanged. The importance of the inversion noise in the turn-on-time statistics is evident: Overall better agreement is obtained with the inversion noise included in the simulation. Laser models often neglect the inversion noise.[29]

Figure 13 shows that the effect of removing the inversion noise is to increase the initial rate of growth of the total and the mode intensities. This is the effect that one would expect in a noise-driven transition from an unstable to a stable equilibrium (e.g., the fall of a ball down a hill into a valley will generally be faster when the early stages of the fall are unperturbed by random kicks), as was pointed out in the context of the laser by, for example, Haake *et al.*[8] Later in the turn-on the effect of omitting the noise is less important.

We decrease the standard deviation of the turn-on times, shown in Fig. 14, by removing the inversion noise, as one might intuitively expect. The effect on the mode intensity turn-on time standard deviation is especially evident early in the turn-on transient. The fact that better agreement is obtained between the simulation and the experimental results for the standard deviation of the total intensity turn-on time with the inversion noise included suggests that even better agreement might be possible if the pump noise (evident in Fig. 4) were included by the simulation.

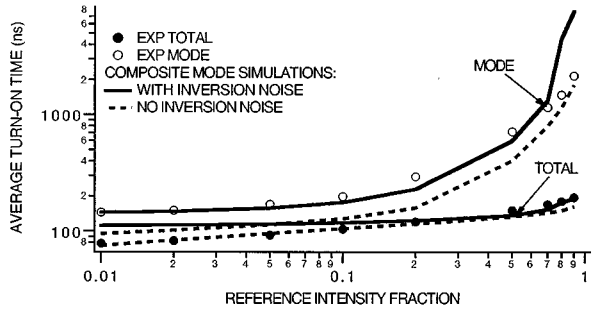

Fig. 13. Comparison of the average turn-on time from the simulation with and without the inversion noise and from the experiment (EXP). Results for the total and the (composite) mode intensities are shown versus the fraction of cw intensity.

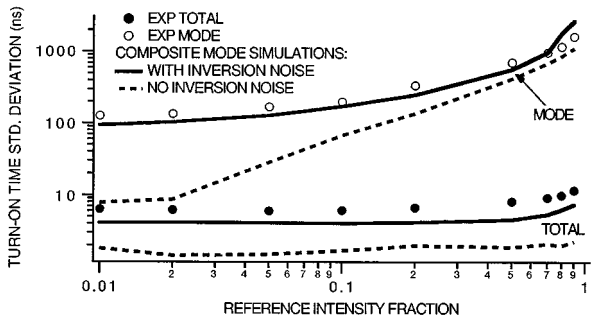

Fig. 14. Comparison of the turn-on time standard deviation from the simulation with and without the inversion noise and from the experiment (EXP). Results for the total and the (composite) mode intensities are shown versus the fraction of cw intensity.

6. CONCLUSION

We have presented experimental and theoretical simulation results that distinguish the turn-on transient dynamical and statistical behavior of the total and longitudinal mode intensities of a multimode compound-cavity laser. The relatively quick turn-on of the total intensity is due to the many (~1000) initial, transient modes with a mode frequency spacing set by the cavity length. Following this rapid rise, a period of much slower redistribution of energy between modes occurs, with the result that the few modes that survive the turn-on transient become cw much more slowly, and with a much larger turn-on time standard deviation, than does the total intensity. During this period of redistribution the total intensity is stable. The redistribution is due to the weak intracavity étalon formed by the dye layer and is manifested by a kink in the growth of mode intensity of modes that become cw.

The numerical model used in the simulation included a large number of modes (91) with the spatial dependence of the mode functions derived for the coupled-cavity geometry used in the experiment. These numerical simulations give good agreement with experimentally determined turn-on time dynamics and statistics throughout the turn-on transient. Our results indicate that the population-inversion fluctuations are significant in describing the statistics of the turn-on transients. The simulations show that the turn-on of individual modes is initially dominated by the stochastic process of spontaneous emission, as the turn-on of the total intensity is, but the mode turn-on is finally dominated by the dynamics of mode competition for the finite reservoir of excited gain centers. The result is that the total intensity and the individual mode intensities evolve in a quite different ways during the turn-on transient of a multimode laser.

ACKNOWLEDGMENTS

The authors gratefully acknowledge useful discussions with Don Adkinson, Mark Beck, Mike Belsley, and Tho-

mas Mossberg. This research was partially funded by the U.S. Department of Energy, the National Science Foundation, the Santa Barbara Research Center, and the U.S. Department of Education.

*Present address, Santa Barbara Dual Spectrum, KIDDE Technologies, Inc., 163 Aero Camino, Goleta, California 93117.

†Present address, Department of Chemistry, University of Warsaw, Warsaw, Poland.

‡Present address, Joint Institute for Laboratory Astrophysics and Department of Physics, University of Colorado at Boulder, Boulder, Colorado 80309.

REFERENCES AND NOTES

1. F. T. Arecchi, A. Politi, L. Ulivi, and V. Degiorgio, "Stochastic-time description of transitions in unstable and multistable systems. I," Nuovo Cimento **71**, 119 (1982); R. Roy, A. W. Yu, and S. Zhu, "Quantum fluctuations, pump noise, and the growth of laser radiation," Phys. Rev. Lett. **55**, 2794 (1985); F. de Pasquale, J. M. Sancho, M. San Miguel, and P. Tartalglia, "Theory for the transient statistics of a dye laser," Phys. Rev. Lett. **56**, 2473 (1986); F. T. Arecchi, W. Gadomski, R. Meucci, and J. A. Roversi, "Dynamics of laser buildup from quantum noise," Phys. Rev. A **39**, 4004 (1989); A. Mecozzi, P. Spano, A. D'Ottavi, and S. Piazzola, "Analysis of transients in pulse modulated semiconductor lasers biased near threshold," Appl. Phys. Lett. **55**, 769 (1989); S. Balle, F. de Pasquale, and M. San Miguel, "Passage-time calculation for the detection of weak signals via the transient dynamics of a laser," Phys. Rev. A **41**, 5012 (1990).
2. S. Zhu, A. W. Yu, and R. Roy, "Statistical fluctuations in laser transients," Phys. Rev. A **34**, 4333 (1986).
3. Two modes: R. Roy, R. Short, J. Durnin, and L. Mandel, "First-passage-time distributions under the influence of quantum fluctuations in a laser," Phys. Rev. Lett. **45**, 1486 (1980); P. Lett, "Investigation of first-passage-time problems in the two-mode dye laser," Phys. Rev. A **34**, 2044 (1986); S. E. Miller, "Turn-on jitter in nearly single-mode injection lasers," IEEE J. Quantum Electron. **QE-22**, 16 (1986); more than two modes: S. E. Miller, and D. Marcuse, "On fluctuations on transients in injection lasers," IEEE J. Quantum Electron. **QE-20**, 1032 (1984); M. M. Choy, P. L. Liu, P. W. Shumate, T. P. Lee, and S. Tsuji, "Measurements of dynamic photon fluctuations in a directly modulated 1.5-mu m InGaAsP distributed feedback laser," Appl. Phys. Lett. **47**, 448 (1985); P. Spano, A. D'Ottavi, A. Mecozzi, and B. Daino, "Experimental observation of time jitter in semiconductor laser turn-on," Appl. Phys. Lett. **52**, 2203 (1988); P. Spano, A. D'Ottavi, A. Mecozzi, B. Daino, and S. Piazzolla, "Experimental measurements and theory of first passage time in pulse-modulated semiconductor lasers," IEEE J. Quantum Electron. **25**, 1440 (1989); P. L. Liu, "Photon statistics and mode partition noise of semiconductor lasers," in *Coherence, Amplification and Quantum Effects in Semiconductor Lasers*, Y. Yamamoto, ed. (Wiley, New York, 1991), Chap. 10, p. 444; A. Mecozzi, A. Sapia, P. Spano, and G. P. Agrawal, "Transient multimode dynamics in nearly single-mode lasers," IEEE J. Quantum Electron. **27**, 332 (1991).
4. S. E. Hodges, M. Munroe, D. Adkison, W. Gadomski, and M. G. Raymer, "Turn-on transient statistics and dynamics in a multimode, short-cavity laser," Opt. Lett. **17**, 931 (1992).
5. S. E. Hodges, "Turn-on transient dynamics in a multimode laser," Ph.D. dissertation (University of Oregon, Eugene, Ore., 1993).
6. I. C. Littler, S. Balle, and K. Bergmann, "Continuous-wave laser without frequency-domain-mode structure: investigation of emission properties and buildup dynamics," J. Opt. Soc. Am. B **8**, 1412 (1991).
7. P. Jung, G. Vemuri, and R. Roy, "Transient dynamics of a laser with an injected signal," Opt. Commun. **78**, 58 (1990); G. Vemuri and R. Roy, "Effect on injected field statistics on transient dynamics of an injection seeded laser," Opt. Commun. **77**, 318 (1990).
8. F. Haake, J. W. Haus, and R. J. Glauber, "Passage-time statistics for the decay of unstable equilibrium states," Phys. Rev. A **23**, 3255 (1981).
9. S. E. Hodges, M. Munroe, J. Cooper, and M. G. Raymer, "A multimode laser model with coupled cavities and quantum noise. I," J. Opt. Soc. Am. B **14**, 191–199 (1997).
10. F. T. Arecchi, V. Degiorgio, and B. Querzola, "Time-dependent statistical properties of the laser radiation," Phys. Rev. Lett. **19**, 1168 (1967); F. T. Arecchi and V. Degiorgio, "Statistical properties of laser radiation during a transient buildup," Phys. Rev. A **3**, 1108 (1971); D. Meltzer and L. Mandel, "Dynamics of a *Q*-switched laser near threshold," Phys. Rev. A **3**, 1763 (1971).
11. D. Marcuse and T. P. Lee, "On approximate analytical solutions of rate equations for studying transient spectra of injection lasers," IEEE J. Quantum Electron. **QE-19**, 1397 (1983); "Rate equation model of a coupled-cavity laser," IEEE J. Quantum Electron. **QE-20**, 166 (1984); S. E. Miller and D. Marcuse, "Computer simulation of laser photon fluctuations: theory of single-cavity laser," IEEE J. Quantum Electron. **QE-20**, 1032 (1984); D. Marcuse, "Computer simulation of laser photon fluctuations: single-cavity laser results," IEEE J. Quantum Electron. **QE-20**, 1139 (1984).
12. E. N. Antonov, V. G. Koloshnikov, and V. R. Mironenko, "Quantitative measurement of small absorption coefficients in intracavity absorption spectroscopy using a cw dye laser," Opt. Commun. **15**, 99 (1975).
13. S. E. Hodges, M. Munroe, J. Cooper, and M. G. Raymer, "Compound-cavity laser modes for arbitrary interface reflectivity," Opt. Lett. **18**, 1481 (1993).
14. The results of this paper are described in the dissertation of S. E. Hodges, referenced above,[5] and extends the preliminary results reported earlier in Ref. 4. In that earlier work a simplified treatment of the coupled-cavity effect on the gain was used, leading to a less quantitative agreement between theory and experiment than is presented here.
15. O. G. Peterson, S. A. Tuccio, and B. B. Snavely, "C. W. operation of an organic dye solution laser," Appl. Phys. Lett. **17**, 245 (1970).
16. T. H. Chyba, E. C. Gage, R. Ghosh, P. Lett, L. Mandel, and I. McMackin, "Chaos in a good-cavity single-mode dye laser due to turbulent dye flow," Opt. Lett. **12**, 422 (1987).
17. A. W. Yu, G. P. Agarwal, and R. Roy, "Noise propagation from pump to secondary lasers," Opt. Lett. **12**, 806 (1987).
18. M. Beck, I. McMackin, and M. G. Raymer, "Transition from quantum-noise-driven dynamics to deterministic dynamics in a multimode laser," Phys. Rev. A **40**, 2410 (1989). Critical slowing, including the onset of relaxation oscillations, in the case of a filled dye laser cavity was observed and simulated and reported in the dissertation of Hodges.[5]
19. E. A. Gavronskaya, A. V. Groznyi, D. I. Staselko, and V. L. Strigun, "Dynamics of thermooptical inhomogeneities in the active medium of an organic dye laser with flash-lamp pumping," Opt. Spectrosc. **42**, 213 (1977); A. V. Aristov, D. A. Kozlovski, D. I. Staselko, and V. L. Strigun, "Acoustooptical distortions induced by pump lamp radiation in ethanol and water dye solutions," Opt. Spectrosc. **45**, 683 (1978).
20. T. F. Johnston, Jr., R. H. Brady, and W. Proffitt, "Powerful single-frequency ring dye laser spanning the visible spectrum," Appl. Opt. **21**, 2307 (1982).
21. Ref. 13; M. H. Rose, M. Lindsey, W. W. Chow, S. W. Koch, and M. Sargent III, "Composite-cavity-mode approach to single-mode semiconductor-laser feedback instabilities," Phys. Rev. A **46**, 603 (1992).
22. M. Munroe, S. E. Hodges, J. Cooper, and M. G. Raymer, "Total intensity modulation and mode hopping in a coupled-cavity laser as a result of external-cavity length variations," Opt. Lett. **19**, 105 (1994).

23. W. H. Press, B. P. Flannery, S. A. Teukolsky, and W. T. Vetterling, *Numerical Recipes* (FORTRAN *Version*) (Cambridge U. Press, Cambridge, 1989), Chap. 13, pp. 455–457.
24. C. W. Gardiner, *Handbook of Stochastic Methods* (Springer-Verlag, Berlin, 1983), Chap. 4, pp. 80–85.
25. J. D. Jackson, *Classical Electrodynamics* (Wiley, New York, 1975), Chap. 7, p. 282.
26. M. Born and E. Wolf, *Principles of Optics* (Pergamon, Oxford, 1980), Chap. 1, p. 66.
27. As one might expect, the Airy formula also describes the annular rings observed in the spatial pattern of the dye-laser output when the external output mirror is replaced by one adjacent to the dye flow, forming a classical étalon. Such a laser system is considered in S. E. Hodges, W. Gadomski and M. G. Raymer, "Observation of Kastler ring emission from a short-cavity laser," Appl. Opt. **32**, 5930 (1993).
28. For example, see O. Svelto, *Principles of Lasers*, 3rd ed. (Plenum, New York, 1989), Chap. 6, pp. 331–339; F. P. Schaefer, ed., *Dye Lasers*, 3rd ed. (Springer-Verlag, Berlin, 1990), Chap. 1, pp. 34, 86–90; F. J. Duarte and L. W. Hillman, eds., *Dye Laser Principles with Applications* (Academic, Boston, Mass., 1990), Chap. 5, p. 195.
29. H. Haken, *Light* (North-Holland, Amsterdam, 1985), Vol. 2, Chap. 10, p. 248.